

Performance comparison among three different Stokes vector direct-detection receivers

Xiaojie Shen (申晓杰)^{1,†}, Jiahao Huo (霍佳皓)^{1,2,†}, Xian Zhou (周 娴)^{1,2,*},
Kangping Zhong (钟康平)³, Jinhui Yuan (苑金辉)², Jiajing Tu (涂佳静)¹,
Keping Long (隆克平)¹, Changyuan Yu (余长源)², Alan Pak Tao Lau (刘伯涛)⁴,
and Chao Lu (吕 超)²

¹Institute of Artificial Intelligence, University of Science and Technology Beijing (USTB), Beijing 100083, China

²Department of Electronic and Information Engineering, The Hong Kong Polytechnic University, Hung Hom, Kowloon, Hong Kong 999077, China

³MACOM Technology Solutions, Shenzhen 518000, China

⁴Department of Electrical Engineering, The Hong Kong Polytechnic University, Hung Hom, Kowloon, Hong Kong 999077, China

*Corresponding author: zhouxian219@gmail.com

Received June 14, 2018; accepted August 31, 2018; posted online September 25, 2018

Stokes vectors direct detection (SV-DD) is an effective solution for short-reach optical communications. In this Letter, we investigate two-dimensional-modulation direct-detection systems based on three Stokes vector receivers (SVRs). The influences of three key factors including the states-of-polarization (SOP), the splitting ratio of the coupler, and the excess loss (EL) are studied in detail. It is shown that the splitting ratio for achieving optimum performance will be changed with SOP and EL conditions. Among these SVRs, the 3×3 coupler-based receiver with its optimal splitting ratio shows the best bit error rate performance and stability against the change of SOP.

OCIS codes: 060.2330, 060.4080, 060.4230.

doi: 10.3788/COL201816.100605.

The development of big data, cloud computing, and other technologies has greatly increased the demand for network traffic^[1]. During the last decade, with the development of coherent communications, long-haul optical networks have achieved terabit per second capacity^[2,3]. However, different from long-haul networks, short-reach applications pay more attention to cost, size, and power efficiency while increasing transmission capacity^[4,5]. Compared to coherent detection (CD), direct detection (DD) is a more cost-effective optical scheme^[6]. Recently, polarization multiplexing with Stokes vectors direct detection (SV-DD) has been studied to further increase data rate. Shieh *et al.* proposed a transmission system scheme of polarization division multiplexing with signal-carrier direct detection (PDM-SC-DD)^[7]. Morsy-Osman *et al.* proposed a polarization division multiplexing intensity modulation with direct detection (PDM-IM-DD) system based on the PAM4 technique^[8]. Examples of typical structures of SV-DD systems can be found in Refs. [9,10]. However, little attention has been paid to the splitting ratio of the coupler and the excess loss (EL) (EL is the ratio of total input power to total output power of optical device) of the 90° optical hybrid and the 3×3 coupler. These parameters need to be considered in order to further improve the performance.

In this Letter, we first review the transmitter and receiver structures of two-dimensional (2D) SV-DD systems, and present the principle of converting the receiving signal to Stokes space. Considering the coupler splitting ratio, we updated three mapping matrices that can map

the receiver signals detected by photodetector (PD) to Stokes space. Then, we assumed that the received signal is mixed with the normalized additive white Gaussian noise (AWGN). We quantitatively analyzed the noise performance of these SV-DD systems by using a channel matrix and mapping matrices, and concluded that the effects induced by the states of polarization (SOP) can be ignored in the case of the specific splitting ratio. Then we performed simulations to verify the above analysis and provide the optimal splitting ratio and system performance of each SV-DD scheme. Finally, we studied the effect of EL of the 90° optical hybrid and the 3×3 coupler. In this case, a higher power cost was necessary to offset the effects of EL for the 90° optical hybrid.

For SV-DD, the transmitted signal can be equivalently represented by a three-dimensional (3D) Stokes vector $S = [S_1, S_2, S_3]^T$, where T denotes the transpose of the vector. The Stokes vector can be defined as

$$\begin{aligned} S_0 &= |E_X|^2 + |E_Y|^2, & S_2 &= 2\text{Re}\{E_X \cdot E_Y^*\}, \\ S_1 &= |E_X|^2 - |E_Y|^2, & S_3 &= 2\text{Im}\{E_X \cdot E_Y^*\}, \end{aligned} \quad (1)$$

where Re and Im stand for the real and imaginary part of a complex variable, respectively, and the asterisk superscript denotes the complex conjugate, while S_0 is given by $S_0 = \sqrt{S_1^2 + S_2^2 + S_3^2}$. Here, for 2D transmission systems, we consider the two popular transmitters shown in Fig. 1. One of the transmitters, shown in Fig. 1(a), sends

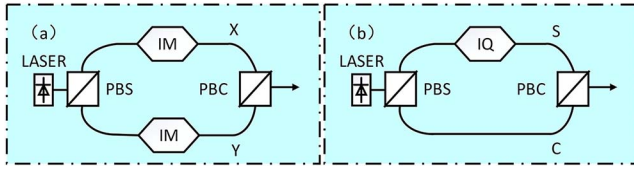


Fig. 1. Structures of SV-DD transmitters: (a) polarization division multiplexing based on intensity modulation and (b) polarization division multiplexing with signal-carrier.

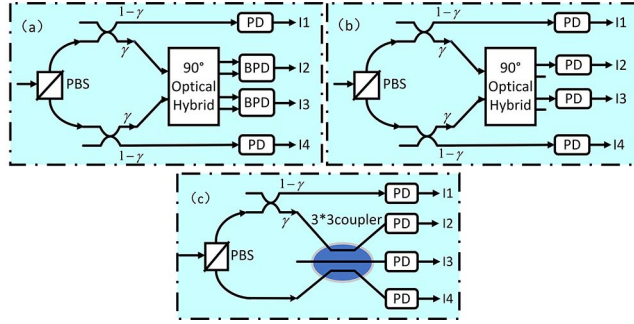


Fig. 2. Structures of SV-DD receivers. (a) Receiver A: with two BPDs, two PDs, and a 90° optical hybrid. (b) Receiver B: with four PDs, and a 90° optical hybrid. (c) Receiver C: with four PDs and a 3 × 3 coupler.

two intensity-modulated (IM) signals on an orthogonal SOP^[11]. The information of the signal is contained in the S_0 and S_1 components. Another transmitter, shown in Fig. 1(b), sends a complex signal (S) in X polarization, while a constant carrier (C) is sent in Y polarization^[12]. The signal information is contained in the S_2 and S_3 components.

Typical receivers of SV-DD are shown in Fig. 2. Receiver A, shown in Fig. 2(a), comprises a polarization beam splitter (PBS), two fiber optic couplers, a 90° optical hybrid, two balanced photodetectors (BPDs), and two PDs^[13]. The PBS splits the received signal into two orthogonal polarizations. Then, the two tributary signals are divided into four signals by the two 2 × 2 optical couplers; here, we assume that the 50/50 couplers are replaced by $\gamma/(1-\gamma)$ couplers. After the 90° optical hybrid, we can detect the front-end output $I = [I_1, I_2, I_3, I_4]^T$ by the PDs. Vector $[S_{R1}, S_{R2}, S_{R3}]^T$ can be straightforwardly acquired by receiver A. In order to further reduce cost, only two outputs of the 90° optical hybrid are detected by two PDs in receiver B, shown in Fig. 2(b), providing the outputs of $|X+Y|^2$ and $|X+iY|^2$. Components S_{R2} and S_{R3} cannot be obtained directly because only two outputs of a 90° optical hybrid are used. Figure 2(c) shows a novel Stokes vector receiver (SVR) with a 3 × 3 coupler^[10].

At the receiver, we can get the output currents of the photodetectors $I = [I_1, I_2, I_3, I_4] + N$, where N denotes the receiver noise. Here, we focus on the un-amplified system dominated by the thermal noise, assuming an additive

Gaussian noise at the receiver $N = [n_1, n_2, n_3, n_4]$ ^[10,14]. The Stokes vector of the receiver S_R can be obtained by

$$S_R = MI, \quad (2)$$

where M is the 4 × 4 mapping matrix given by

$$\begin{aligned} M_1 &= \begin{bmatrix} \frac{1}{1-\gamma} & 0 & 0 & \frac{1}{1-\gamma} \\ \frac{1}{1-\gamma} & 0 & 0 & -\frac{1}{1-\gamma} \\ 0 & \frac{2}{\gamma} & 0 & 0 \\ 0 & 0 & \frac{2}{\gamma} & 0 \end{bmatrix}, M_2 \\ &= \begin{bmatrix} \frac{1}{1-\gamma} & 0 & 0 & \frac{1}{1-\gamma} \\ \frac{1}{1-\gamma} & 0 & 0 & -\frac{1}{1-\gamma} \\ -\frac{1}{1-\gamma} & \frac{4}{\gamma} & 0 & -\frac{1}{1-\gamma} \\ -\frac{1}{1-\gamma} & 0 & \frac{4}{\gamma} & -\frac{1}{1-\gamma} \end{bmatrix}, M_3 \\ &= \begin{bmatrix} 1 & 1 & 1 & 1 \\ \frac{2}{1-\gamma} - 1 & -1 & -1 & -1 \\ 0 & -\sqrt{\frac{2}{\gamma}} & 0 & \sqrt{\frac{2}{\gamma}} \\ 0 & \frac{1}{\sqrt{\gamma}} & -\frac{2}{\sqrt{\gamma}} & \frac{1}{\sqrt{\gamma}} \end{bmatrix}, \end{aligned} \quad (3)$$

where M_1 , M_2 , and M_3 are the mapping matrices of receivers A, B, and C, respectively. S_R is obtained by using the front-end output I . The noise is mapped to the Stoke space as $N_S = MN$. In Stokes space, the transfer equation can be written as

$$S_R = HS_T + N_S, \quad (4)$$

where S_T is the SV of the transmitter, N_S is an additive noise vector, and H is the channel matrix. In this case, for simplicity, only a random polarization rotation is considered in the following theoretical derivations. Matrix H can be expressed by a Muller matrix

$$H = \begin{bmatrix} 1 & 0 & 0 & 0 \\ 0 & \cos 2\phi & -\sin 2\phi & 0 \\ 0 & \sin 2\phi & \cos 2\phi & 0 \\ 0 & 0 & 0 & 1 \end{bmatrix}, \quad (5)$$

where ϕ denotes the random polar angles. The Muller matrix H can be determined by pilot-aided or blind channel estimation^[15,16], and as the receiver has instantaneous knowledge of H , it reverses the channel effect to obtain

$$\tilde{S}_T = H^{-1}HS_T + H^{-1}N_S = S_T + \tilde{N}, \quad (6)$$

where \tilde{S}_T is the approximate Stokes vector that we can calculate from output currents of the photodetectors, and noise vector \tilde{N} undergoes the same transformation process, which can be expressed as

$$\tilde{N} = H^{-1}N_S = H^{-1}MN. \quad (7)$$

As can be seen from Eq. (7), the receiver noise is changed with the mapping and channel estimation process

when the data is recovered. Here, we use the SV-DD system with receiver A as an example to illustrate the variations of noise. By substituting H^{-1} and M_1 into Eq. (7), \tilde{N} can be written as

$$\begin{aligned} \tilde{N} &= H^{-1}MN \\ &= \begin{bmatrix} 1 & 0 & 0 & 0 \\ 0 & \cos 2\phi & -\sin 2\phi & 0 \\ 0 & \sin 2\phi & \cos 2\phi & 0 \\ 0 & 0 & 0 & 1 \end{bmatrix}^{-1} \\ &\quad \times \begin{bmatrix} \frac{1}{1-\gamma} & 0 & 0 & \frac{1}{1-\gamma} \\ \frac{1}{1-\gamma} & 0 & 0 & -\frac{1}{1-\gamma} \\ 0 & \frac{2}{\gamma} & 0 & 0 \\ 0 & 0 & \frac{2}{\gamma} & 0 \end{bmatrix} \times \begin{bmatrix} n_1 \\ n_2 \\ n_3 \\ n_4 \end{bmatrix}. \end{aligned} \quad (8)$$

It is apparent from Eq. (8) that the noise is related to the received ϕ of the SOP and the splitting ratio γ , where we omit the dispersion-related effects. For the PDM-IM systems, shown in Fig. 1(a), the intensity of the two polarizations is contained in S_{T0} and S_{T1} . As can be seen from Eq. (6), \tilde{S}_{T0} and \tilde{S}_{T1} are related to \tilde{n}_1 and \tilde{n}_2 , respectively. Therefore, \tilde{n}_1 and \tilde{n}_2 have an important effect on the PDM-IM system. The noise performance of the system can be demonstrated by a superposition of \tilde{n}_1 and \tilde{n}_2 . Figure 3 shows the average noise power as a function of γ for different received SOPs. Noise power is normalized with respect to n_1 and measured in decibels.

Here, we selected five SOPs (0° , 22.5° , 45° , 67.5° , and 90°), and demonstrated the effect of the splitting ratio, as shown in Fig. 3. It is apparent that the SOPs are symmetrically distributed around 45° ; the curves of the 0° and 90° SOPs and the curves of the 22.5° and 67.5° SOPs are essentially the same. In addition, as shown in Fig. 3(a), the noise performance becomes completely independent from SOP for receiver A when $\gamma = 0.667$ (SOP independent

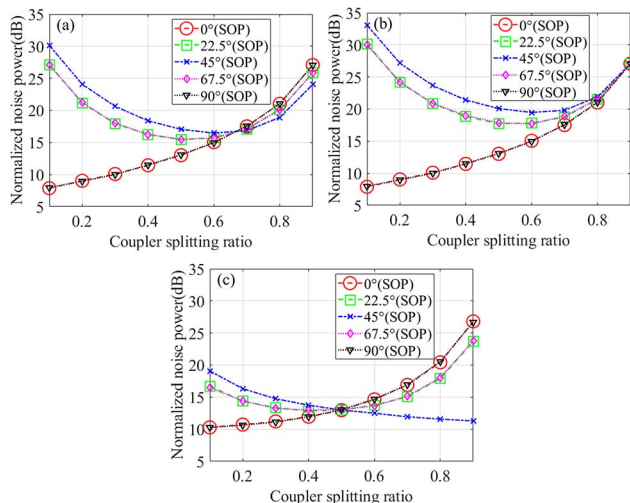


Fig. 3. Normalized noise power as a function of the coupler splitting ratio of the PDM-IM: (a) for receiver A, (b) for receiver B, and (c) for receiver C.

splitting ratio). For receiver B, the noise performance gradually approaches when $\gamma > 0.8$. For receiver C, the noise performance becomes completely independent of the SOP when $\gamma = 0.5$. Furthermore, when the SOPs are 0° and 90° , the noise performance is much better than that of other SOPs for receivers A and B. As can be seen from the polarization rotation matrix, S_0 and S_3 obviously do not vary with the SOP. Nevertheless, S_1 and S_2 can be transformed between each other by varying the SOP. When the SOPs are 0° and 90° , \tilde{S}_{T1} can be obtained by using S_{R1} only. When the SOP is 45° , \tilde{S}_{T1} is completely given by S_{R2} , while in other cases, S_{R1} and S_{R2} need to be used. For the PDM-IM system, the intensity information is contained in S_0 and S_1 ; thus, S_{R0} , S_{R1} , and S_{R2} are necessary components. When γ is reduced below $2/3$, more power is allocated to I_1 and I_4 in receivers A and B. As can be seen from Eq. (2) and M_1 , S_{R0} and S_{R1} are given by I_1 and I_4 , respectively. This results in a much better performance when the SOP is close to 0° and 90° .

For the PDM-SC systems, shown in Fig. 1(b), the complex signal is contained in S_2 and S_3 . Therefore, \tilde{n}_3 and \tilde{n}_4 have an important effect on the PDM-SC system. Figure 4 shows the average noise power as a function of γ for different received SOPs.

Like above, the noise performance is affected by the γ and the SOP. As shown in Figs. 4(a) and 4(c), the noise performance becomes completely independent of the SOP when $\gamma = 0.667$ and $\gamma = 0.5$. In contrast, the information of the PDM-SC signal is contained in S_2 and S_3 ; thus, the curve is apparently symmetric with respect to the curve in Fig. 3.

The simulation model for the proposed system is built by VPI transmission Maker 8.7 and MATLAB software. At the transmitter, as shown in Fig. 1, PAM4 and 16QAM signals are selected to simulate PDM-IM and PDM-SC systems, respectively. The transmission rate of the signal

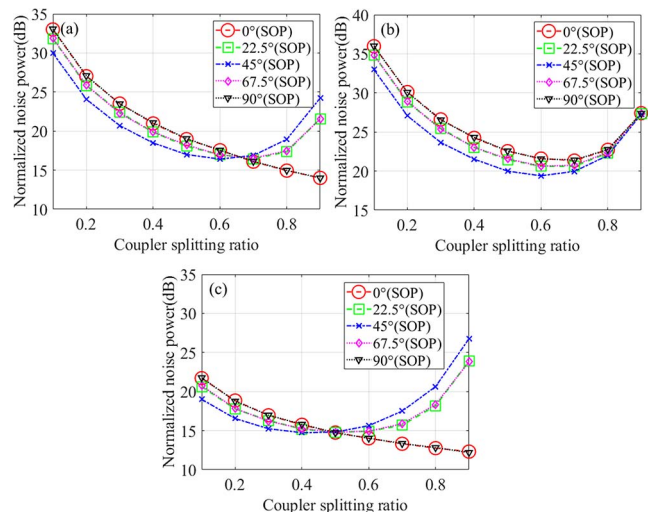


Fig. 4. Normalized noise power as a function of the coupler splitting ratio of the PDM-SC: (a) for receiver A, (b) for receiver B, and (c) for receiver C.

Table 1. General Simulation Parameters of 112 Gbit/s PDM-DD Systems

Parameter	Values	Parameter	Values
Baud	28 Gbaud	DAC/ADC rate	56 GSam/s
Laser linewidth	5 MHz	PD responsibility	0.65 A/W
Laser RIN	-160 dB/Hz	PD thermal noise	20 pA/Hz ^{0.5}
TX/RX bandwidth	20 GHz	PD dark current	10 nA

is set to 112 Gbit/s. Table 1 summarizes the general settings of the simulation parameters.

In addition to the parameters mentioned above, the shot noise is also considered in the simulation for the PDM-PAM4 system. The structure of the transmitter is shown in Fig. 1(a), and three receivers are shown in Fig. 2. It can be obviously seen in Figs. 5(a)–5(c) that the system performance is very close to the theoretical noise performance. The coupler splitting ratio and the SOP affect the system performance appropriately. The system performance becomes completely independent of the SOP when $\gamma = 0.667$ and $\gamma = 0.5$ for receivers A and C, respectively. For receiver B, the bit error rate (BER) performances converge to each other at $\gamma = 0.8$. Figure 5(d) shows the back-to-back (BTB) BER as a function of received power for three SVRs, where all examined cases are plotted at the optimum coupler splitting ratio. The received optical power (ROP) of the three SVRs are -6.8 dBm, -5.7 dBm, and -8.4 dBm at 7% forward error correction

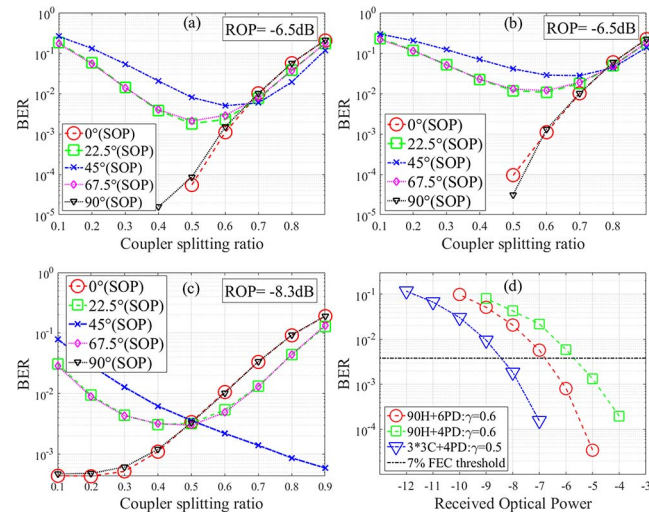


Fig. 5. Simulation results for the PDM-IM system: (a) BER vs. coupler splitting ratio for different SOPs for receiver A, (b) BER vs. coupler splitting ratio for different SOPs for receiver B, (c) BER vs. coupler splitting ratio for different SOPs for receiver C, and (d) BER vs. received optical power for different SVRs in BTB transmissions.

(FEC) threshold. Compared with receiver A, receiver C has a better ROP sensitivity by 1.6 dB.

For the PDM-SC-16-QAM system, the structure of the transmitter is shown in Fig. 1(b) and three receivers are shown in Fig. 2. The carrier-to-signal power ratio (CSPR) is 0 dB. The system performance becomes completely independent of the SOP when $\gamma = 0.667$ and $\gamma = 0.5$ for receiver A and receiver C, as shown in Fig. 6. For receiver B, it can be obviously seen that the optimal performance is achieved when $\gamma = 0.7$. As shown in Fig. 7(d), the ROPs of the three SVRs are -8.7 dBm, -6.6 dBm, and -9.6 dBm

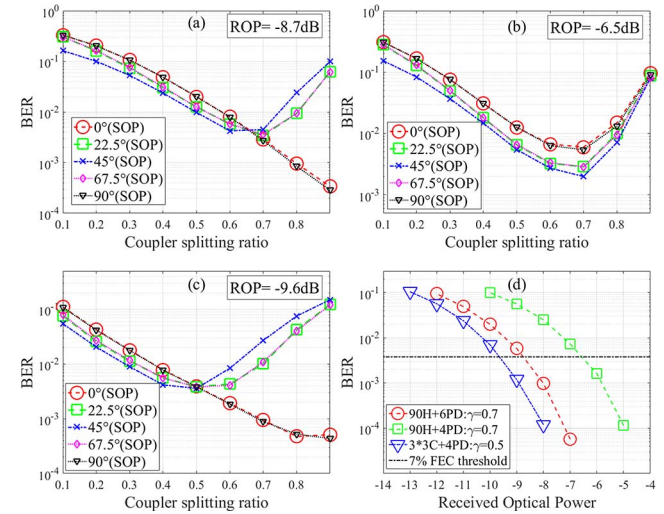


Fig. 6. Simulation results for the PDM-SC system: (a) BER vs. coupler splitting ratio for different SOPs for receiver A, (b) BER vs. coupler splitting ratio for different SOPs for receiver B, (c) BER vs. coupler splitting ratio for different SOPs for receiver C, and (d) BER vs. ROP for different SVRs in BTB transmissions.

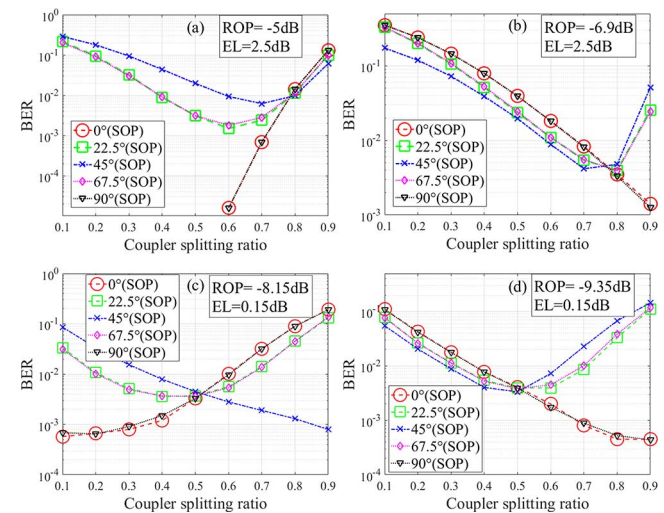


Fig. 7. Simulation results with 2.5 dB EL for the 90° hybrid and 0.15 dB EL for the 3 × 3 coupler: BER vs. coupler splitting ratio for different SOPs (a) for receiver A for the PDM-IM system, (b) for receiver A for the PDM-SC system, (c) for receiver C for the PDM-IM system, and (d) for receiver C for the PDM-SC system.

Table 2. Comparison of 112 Gbit/s PDM-PAM4 and PDM-SC Signals with Different SV-DD Receivers. IM: Intensity Modulation; I/Q: I/Q Modulator; BPD: Balanced Photodetector

System Scheme	Transmitter	Receiver	EL	Optimum splitting ratio	SOP independent splitting ratio	ROP sensitivity (@BER 3.8×10^{-3})
PDM-PAM4-DD (hybrid)	$2 \times$ IM	2PD + 2BPD	No	0.6	0.667	-6.8 dBm
PDM-PAM4-DD (hybrid)	$2 \times$ IM	4PD	No	0.7	-	-5.7 dBm
PDM-PAM4-DD (3×3 coupler)	$2 \times$ IM	4PD	No	0.5	0.5	-8.4 dBm
PDM-SC-16QAM-DD (hybrid)	$1 \times$ I/Q	2PD + 2BPD	No	0.7	0.667	-8.7 dBm
PDM-SC-16QAM-DD (hybrid)	$1 \times$ I/Q	4PD	No	0.7	-	-6.6 dBm
PDM-16QAM-DD (3×3 coupler)	$1 \times$ I/Q	4PD	No	0.5	0.5	-9.6 dBm
PDM-PAM4-DD (hybrid)	$2 \times$ IM	2PD + 2BPD	Yes (2.5 dB)	0.7	0.8	-5 dBm
PDM-SC-16QAM-DD (hybrid)	$1 \times$ I/Q	2PD + 2BPD	Yes (2.5 dB)	0.8	0.8	-6.9 dBm
PDM-PAM4-DD (3×3 coupler)	$2 \times$ IM	4PD	Yes (0.15 dB)	0.5	0.5	-8.15 dBm
PDM-16QAM-DD (3×3 coupler)	$1 \times$ I/Q	4PD	Yes (0.15 dB)	0.5	0.5	-9.35 dBm

at 7% FEC threshold. Compared with receiver A, receiver C has a better ROP sensitivity by 0.9 dB.

In the previous simulation, we only considered the receiver noise, the coupler splitting ratio, and the SOP. Here, we present the results to further investigate the effect of EL on the system performance by simulation. The EL of the 90° hybrid is smaller than 2.5 dB, which is obtained by the datasheet of the commercial 90° hybrid (Kyliya COH24). The EL of the 3×3 coupler is 0.15 dB, which is obtained by the datasheet of the commercial 3×3 coupler (Phoenix V1_0603). In this part of the simulation, we assume a 2.5 dB EL for the 90° hybrid and 0.15 dB EL for the 3×3 coupler.

Figures 7(a) and 7(b) show the BER performance as a function of the coupler splitting ratio with the 2.5 dB EL of the 90° hybrid. It can be obviously seen that the BER performance is independent of SOP when $\gamma \approx 0.8$ for both the PDM-IM and the PDM-SC systems using receiver A. The PDM-IM system using receiver A achieves a system BER below the 7% FEC threshold BER when $\gamma = 0.7$, as shown in Fig. 7(a). We can conclude that 2.5 dB EL results in an ROP sensitivity penalty of ~ 1.8 dB. For the PDM-SC system, the optimum coupler splitting ratio is $\gamma = 0.8$ and the 2.5 dB EL results in an ROP sensitivity penalty of ~ 1.8 dB. The input of the 90° hybrid requires more output to offset the power decline resulting from the EL. By selecting the appropriate optical coupler, the performance attenuation resulting from the EL can be reduced. For the 3×3

coupler-based SV-DD receivers, as shown in Figs. 7(c) and 7(d), the 0.15 dB EL results in an ROP sensitivity penalty of 0.25 dB for both the PDM-IM and the PDM-SC systems. The optimum coupler splitting ratio is maintained at $\gamma = 0.5$. Table 2 summarizes and compares the 112 Gbit/s PDM-PAM4 and PDM-SC systems with different SV-DD receivers.

In this Letter, we studied the performances of the PDM-PAM4 and PDM-SC-16QAM signals using three different SV-DD receivers. In terms of system performance, the three crucial factors are the coupler splitting ratio, the SOP, and EL. In the 90° optical hybrid-based SV-DD receiver, the coupler with a 60/40 or 70/30 splitting ratio exhibits a better ROP performance than that with a splitting ratio of 50/50, especially for PDM-SC systems. It should be noted that the performance was completely independent of the SOP when a 67/33 coupler was used. Considering the 90° optical hybrid with a common EL of 2.5 dB, the 80/20 coupler achieved a steady performance independent of the SOP. In this case, there were receiver sensitivity penalties of 1.8 dB for both the PDM-IM and the PDM-SC systems. When 3×3 coupler-based SV-DD receivers were used, the best performance could be reached with a coupler splitting ratio of 50/50. Compared to receiver A, the PDM-IM and PDM-SC signals had better receiver sensitivities by 1.6 dB and 0.9 dB, respectively. Therefore, a cost-efficient 3×3 coupler-based SV-DD receiver is a promising choice for PDM-DD signals.

This work was supported by the National Natural Science Foundation of China (Nos. 61671053, 61871030, and 61435006), the Fundamental Research Funds for the Central Universities (No. FRF-BD-17-015A), the Foundation of Beijing Engineering and Technology Center for Convergence Networks and Ubiquitous Services, the State Key Laboratory of Advanced Optical Communication Systems Networks, China, the Hong Kong Polytechnic University (Nos. 1-ZVGB, G-SB65, and 4-BCCK), and the RGC of Hong Kong SAR Government (No. 152248/15E).

[†]These authors contributed equally to this work.

References

1. L. Paraschis, in *European Conference and Exhibition on Optical Communication* (2013), paper Th.2.F.3.
2. C. Zhao, Y. Chen, S. Zhang, J. Li, F. Zhang, L. Zhu, and Z. Chen, *Opt. Express* **20**, 787 (2012).
3. L. Cheng, Z. Li, Y. Yang, and C. Lu, in *Optoelectronics and Communications Conference* (2009), paper ThLP80.
4. K. Zhong, X. Zhou, J. Huo, C. Lu, and A. P. T. Lau, *J. Lightwave Technol.* **36**, 377 (2018).
5. S. C. J. Lee, S. Randel, F. Breyer, and A. M. Koonen, *Photon. Technol. Lett.* **21**, 1749 (2009).
6. M. S. Moreolo, J. Fabrega, F. J. Vilchez, L. Nadal, and G. Junyent, in *European Conference and Exhibition on Optical Communication* (2012), paper P3.17.
7. W. Shieh and D. Che, *Proc. SPIE* **10130**, 101300G (2017).
8. M. Morsy-Osman, M. Chagnon, M. Poulin, S. Lessard, and D. V. Plant, in *European Conference on Optical Communication* (2014), paper PD.4.4.
9. D. Che, Q. Hu, and W. Shieh, in *European Conference on Optical Communication* (2015), paper 0887.
10. W. Shieh, H. Khodakarami, and D. Che, *APL Photonics* **1**, 040801 (2016).
11. K. Zhong, X. Zhou, Y. Gao, W. Chen, J. Man, L. Zeng, A. P. T. Lau, and C. Lu, *Photon. Technol. Lett.* **27**, 1757 (2015).
12. D. Che, Q. Hu, and W. Shieh, *J. Lightwave Technol.* **34**, 516 (2016).
13. D. Che, A. Li, X. Chen, Q. Hu, Y. Wang, and W. Shieh, in *Optical Fiber Communications Conference and Exhibition* (2014), paper Th5C.7.
14. X. Zhou, K. Zhong, J. Huo, J. Yuan, F. Li, L. Wang, K. Long, A. P. T. Lau, and C. Lu, *IEEE Photon. J.* **7**, 7802812 (2017).
15. Q. Zhang, Y. Yang, Q. Xiang, Q. He, and Y. Yao, in *Opto-Electronics and Communications Conference (OECC) and Photonics Global Conference (PGC)* (IEEE) (2017), p. 1.
16. D. Che, A. Li, and W. Shieh, in *European Conference on Optical Communication* (2015), paper 0240.